

Landslides (2024) 21:1531–1547  
 DOI 10.1007/s10346-024-02242-8  
 Received: 11 October 2023  
 Accepted: 8 March 2024  
 Published online: 8 April 2024  
 Author(s) 2024

Clàudia Abancó  · Flavio Alexander Asurza  · Vicente Medina  ·  
 Marcel Hürlimann  · Georgina L. Bennett 



## Modelling antecedent soil hydrological conditions to improve the prediction of landslide susceptibility in typhoon-prone regions

**Abstract** Most regional landslide susceptibility models do not consider the evolving soil hydrological conditions leading up to a multiple occurrence regional landslide event. This results in inaccurate predictions due to the non-linear behaviour of the terrain. To address this, we have developed a simple and efficient model that incorporates the mid-term evolution of soil hydrological conditions. The model combines a water balance model and a geotechnical model based on infinite slope theory. The analysis of 561 high-intensity rainfall events in a typhoon-prone region of the Philippines revealed that the percolation of water during the 5-month wet season is crucial in determining landslide susceptibility. Consequently, high-intensity rainfall events at the start of the wet season are less likely to trigger landslides, while later events are more hazardous. We analysed the change in landslide susceptibility during the 2018 rainy season by comparing the probability of failure (PoF) before and after three high-intensity rainfall events (July, August and September). Only the event in September caused a significant increase in the probability of failure (PoF). The model showed an accuracy of 0.63, with stable cells better represented than unstable cells. The antecedent hydrological conditions on the lower soil layers are responsible for changes in landslide susceptibility. Our findings support the hypothesis that new approaches to developing hydro-meteorological thresholds for landslide early warning systems should be evaluated, especially in regions with strong seasonality.

**Keywords** Landslides · Rainfall · Soil moisture · Susceptibility · Typhoon

### Introduction

Rainfall-triggered landslides occur in mountainous areas around the world and have a relevant presence in tropical countries or those affected by extreme meteorological conditions (Kirschbaum et al. 2015; Lin et al. 2017; Froude and Petley 2018). Some of these landslides occur in the form of multiple, almost simultaneous, shallow slope failures, the so-called MORLEs (Multiple Occurrence Regional Landslide Events) according to Crozier (2005). Extreme rainfall events such as tropical cyclones or convective storms are common triggers for MORLEs, which consequences can be devastating, including a great number of fatalities and damage to infrastructure and properties (e.g. Chiang and Chang 2011; Zhuang et al. 2022). Many efforts have been put in the assessment of the hazard and risk associated to MORLEs, mostly relying on the recognition of locations prone to slope instability (Guzzetti et al. 2005; Crozier 2017; Guzzetti 2021) and the identification of critical

rainfall intensities that trigger these instabilities (Guzzetti et al. 2012; Gariano and Guzzetti 2016; Melillo et al. 2018; Reichenbach et al. 2018; Guzzetti 2021). Nevertheless, understanding why the response of the terrain is not linear and MORLEs do not occur always under the same rainfall conditions is still a major challenge (Jones et al. 2021). Observations from typhoon-prone regions (such as the one in this paper) reveal that very similar rainfall conditions at different times may or may not result in MORLEs, this being a key point of this research.

Landslide susceptibility models determine the probability of spatial occurrence of slope failures given a set of geoenvironmental conditions (Guzzetti et al. 2005, 2006). Probability is assessed using data-driven correlations (Baeza and Corominas 2001; Guzzetti et al. 2005; Reichenbach et al. 2018; Hearn and Hart 2019; Lombardo et al. 2019) or physical laws (e.g. Medina et al. 2021; Montgomery & Dietrich 1994) taking terrain characteristics and environmental conditions as input. Although terrain characteristics are nearly static variables (predisposing factors), environmental conditions are controlled by dynamic processes at different time scales (predisposing and triggering factors). Most regional-scale landslide susceptibility models are “single event models” (SEM) and account only for triggering factors that occur on a short timescale, i.e. the rainfall occurred on the day(s) of the MORLE. The reason for this is the computational cost of using longer timescales in large areas. However, it is known that long-term variations of pore-water pressure in the soil due to water infiltration strongly control the instability of the slopes (Iverson 2000; Fan et al. 2020; Pelascini et al. 2022; Napolitano et al. 2016; Tufano et al. 2021); thus, in many occasions, SEM do not perform well as the transient nature of pore-water pressure is overlooked. To overcome such limitation, some SEM include antecedent conditions, such as antecedent rainfall (Crozier and Eyles 1980; De Vita and Piscopo 2002; Glade et al. 2000; Medina et al. 2021, Kirschbaum and Stanley 2018), soil saturation (Leonarduzzi et al. 2021) or soil water content (Crozier 1999).

Remote and in situ sensing are popular alternatives to quantify continuous soil wetness for landslide risk assessment purposes (Wicki et al. 2021). In situ soil moisture sensors are used in early warning systems (Mirus et al. 2018a; Wicki et al. 2020; Oorthuis et al. 2023) to improve traditional rainfall thresholds. Soil moisture satellite measurements are gradually becoming a popular alternative (Brocca et al. 2008; Abraham et al. 2020; Bordoni et al. 2021; Stanley et al. 2021) as their spatial/temporal accuracy increases. A main advantage of using sensing data over modelled data is that it can be used in “continuous models” (CM), where the transient character of the environmental conditions is included. However,

sensing data are not exempt from limitations, and the spatial resolution is amongst the main ones. In situ sensing provides data from specific points that may not be spatially representative. While satellite soil moisture data provides data from a planimetric grid, data sensed from the satellites is only of the very shallow layer of the soil (< 100 cm).

Many tropical areas are characterized by a strong seasonality, with a wet and a dry season, generally due to the impact of monsoons. Typhoons (how tropical cyclones are called in the North-West Pacific region) are very common MORLE triggers (Chiang and Chang 2011; Zhuang et al. 2022). They often occur between June and November, peaking in September, coinciding with the end of the wet season in several Pacific regions (Basconcillo and Moon 2021). The wetness of the soil when typhoons make landfall can be very high, which may result in a higher probability of landslide occurrence. It is, therefore, important to account for the soil wetness when assessing landslide hazard. Higher (lower) water content in the soil pores corresponds to lower (higher) suction on them (van Genuchten 1980). Suction plays a crucial role in partially saturated soils, as it conditions the mechanical behaviour of the soils, and therefore, their stability (Alonso et al. 1990). The seasonality of the weather can, therefore, be associated to a seasonality of slope stability, which should be considered on the regional landslide hazard assessment. Nevertheless, many regional landslide susceptibility models assume the fully saturated soil hypothesis since including the hydrology and mechanics of unsaturated soils is often data demanding and computationally expensive (Baum et al. 2008; Ma et al. 2021).

Focusing on the region of Itogon in the Philippines, which is commonly hit by typhoons and has an extensive history of landslides, we assess the role of antecedent hydrological conditions in the landslide susceptibility models. A recent study of Jones et al. (2023) in this region found that typhoon-triggered landslides in the Philippines display some degree of time dependency, which suggests that they may be affected by the antecedent wetness conditions. Also, in the same region, Abancó et al. (2021) pointed out that the soil saturation of the upper soil layer seemed very relevant for the time of the MORLE occurrence; however, this needs to be proven. Nolasco-Javier and Kumar (2018) developed a minimum rainfall threshold for rainfall-triggered landslides in an adjacent area. They found out that events happened only after 500 mm of antecedent rainfall along the rainy season and suggested that antecedent rainfall does not have a high influence on landslide triggering for short periods (up to 25 days). However, the antecedent rainfall gains importance on the landslide triggering if longer periods are considered. In conclusion, attempts to include long antecedent conditions have been made in the Philippines, but there is a lack of simple, usable models that include these effects in the regional landslide susceptibility assessment.

Here we investigate why regions regularly impacted by typhoons have a different slope stability response under similar triggering rainfall conditions (and the same geologic/geomorphologic predisposing factors). To do so, we have coupled two physically based models and applied them in a landslide-prone region of the Philippines: a water balance model, specifically developed for the context of tropical regions, and the FSLAM landslide susceptibility model (Medina et al. 2021; Guo et al. 2022). The goals of this study focus on the following: (i) quantifying the infiltration of rainfall into the soil for a 20 years

data series; (ii) empirically comparing rainfall and infiltration patterns that caused MORLEs and others that did not; (iii) analysing the landslide susceptibility changes at the event and seasonal timescales. In the Discussion, we also evaluate uncertainties derived from the use of satellite-based soil moisture data in regional slope stability models.

### Study area

Landslides triggered by extreme weather patterns cause severe damage and life losses in the Philippines every year (Nolasco-Javier et al. 2015; Paringit et al. 2020; Abancó et al. 2021; Emberson et al. 2022; Jones et al. 2023). The country has an average annual rainfall of approximately 2348 mm, with more than 4000 mm in the rainiest area (Central Luzon) (Climate Change Knowledge Portal for Development Practitioners and Policy Makers). The rainfall regime is characterized by two monsoon seasons: (a) the southwest monsoon (SWM), from May to September, when the western coast experiences its rainy season and accounts for approximately 43% of the annual rainfall of the country (Asuncion and Jose 1980); and (b) the northeast monsoon (NEM), when the rain hits mostly the eastern coast between October and late March. Besides the monsoons, approximately 20 tropical cyclones enter the Philippine Area of Responsibility, and seven to eight make landfall every year (Nolasco-Javier and Kumar 2019). During the SWM, heavy rain hits the west of the major island of the Philippines, Luzon, which has a very mountainous topography, with half of the island above 500 m.a.s.l. The heavy rainfall, enhanced by the passage of tropical cyclones over the island, triggers a great number of landslide events.

We selected part of the Upper Agno catchment as a study area, in the northwest of the major island of the Philippines, Luzon. The study area contains four sub catchments on the west of the Agno River, at the mining area of Itogon, near the city of Baguio. The region is located at the southern end of the Central Cordillera Mountains. The key reason for selecting these four sub catchments is that they were severely impacted by Typhoon Parma in 2009 (locally known as Typhoon Pepeng) (Nolasco-Javier and Kumar 2018) and Typhoon Mangkhut (locally known as Typhoon Ompong) in 2018 (Abancó et al. 2021), which caused MORLEs in the area (Fig. 1).

The sub catchments under study have areas between 16 and 88 km<sup>2</sup>, with a total area of 200 km<sup>2</sup>, and elevations between 490 and 2018 m above the sea level (m.a.s.l.). The slopes range from flat to 72°, with a mean value of 29°. The catchments are dominated by fine material, from the Bakakeng clay formation and fine-sandy material, from the Ambassador silt formation (Carating et al. 2014).

Landslide inventories from Typhoon Parma (Jones et al. 2023) and Typhoon Mangkhut (Abancó et al. 2021) have been used to calculate the landslide density after each typhoon. More details of the inventories are given in the “Landslide inventories” section. The two most southern sub catchments were covered by the two inventories and were severely impacted in both typhoons, with landslide densities up to 95 and 46 landslides, respectively, in a 500 m radius.

### Data

In the following sections, we present key information on the datasets used as input for an empirical analysis of the landslide-triggering rainfalls and infiltration patterns, as well as for the physically-based models discussed above.

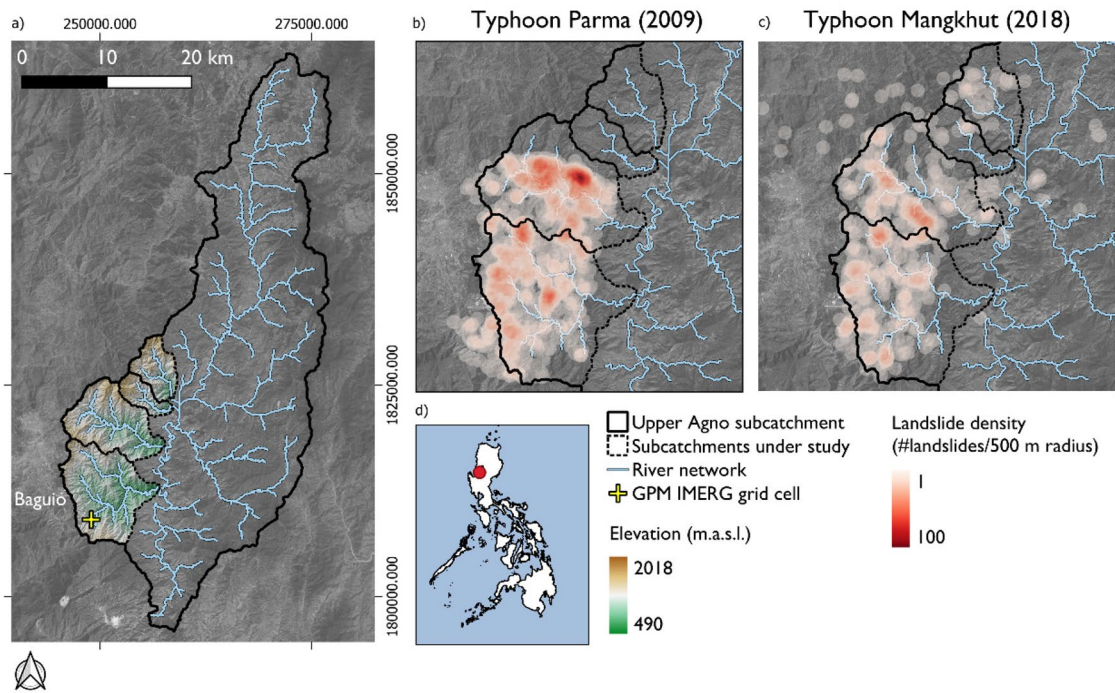


**Fig. 1** Location of the four sub catchments under study within the Upper Agno catchment (a) and location of the Upper Agno catchment within the Philippines (d). Landslide density (number of landslides in a 500 m radius) is indicated for Typhoon Parma (2009) (b) and Typhoon Mangkhut (2018) (c). Note that the Parma inventory only refers over the two southern catchments

## Landslide inventories

We selected a period of 19 years (2001–2020) and researched how MORLEs have impacted the study area. According to the records of the City Disaster Risk Reduction and Management Council (CDRRMC) of the City of Baguio (Paringit et al. 2020), at least 18 tropical cyclones are known to have caused landslides in the area along this period. For most of them, the damage was local or only a few landslides were reported. However, for 2009 and 2018 typhoon events, the number and spatial distribution of landslides was greater and landslide inventories were compiled using satellite imagery (Abancó et al. 2021; Jones et al. 2023). Landslide inventories for the remaining 16 typhoons were not available during this study (Fig. 2).

Most of the landslide-triggering typhoons occurred between July and October, therefore at the end of the SWM season (Fig. 3). Typhoon Parma (called Typhoon Pepeng in the Philippines) was simultaneous to Typhoon Melor (Typhoon Quedan). They created the Fujiwhara effect (or interaction), a relative counterclockwise motion and decreasing separation distance between the two storm centres. Because of the presence of Melor, Parma slowed down and looped, reversed and made landfall three times over northern Luzon (Nolasco-Javier et al. 2015) between 3 and 9 October 2009. The landslide inventory for Typhoon Parma covers the two Southern sub catchments of the study area (Jones et al. 2023). Typhoon Mangkhut, in 2018, crossed the north of Luzon Island between the 13 and 15 of September 2018 along the four sub catchments (Abancó et al. 2021; Jones et al. 2023).

## Digital elevation model

We used a nationwide Digital elevation model (DEM) acquired in 2013 and generated through airborne IfSAR technology with 5-m spatial resolution and 1-m root-mean-square error vertical accuracy (Grafil and Castro 2014) (Fig. 1).

The DEM was used for the physically based model to assess both the hydrological response of the terrain to the rainfall and the landslide susceptibility. This latest is assessed by pixel, so with a 5-m resolution (see results in the “Landslide susceptibility assessment” section).

## Soil

The soil map was provided by the Department of Agriculture-Bureau of Soils and Water Management (DA-BSWM) (Carating et al. 2014). It originally had 15 classes in the study area. They have been reclassified into four broader classes, according to available descriptions (Fig. 6a). The geological origin of the soils was also considered during the reclassification, on the basis of the Geology Map (Baguio City Quadrangle, Sheet 3169 III (DENR-MGB 1995) and the Sison Quadrangle, Sheet 3168 IV (DENR-MGB 2000)), provided by the Department of Environment and Natural Resources’ Mines and Geosciences Bureau (DENR-MGB). Table 1 shows the geotechnical properties of the four classes that are required for the stability analysis. The model used for the slope stability analysis is explained in detail in the “Methods” section.

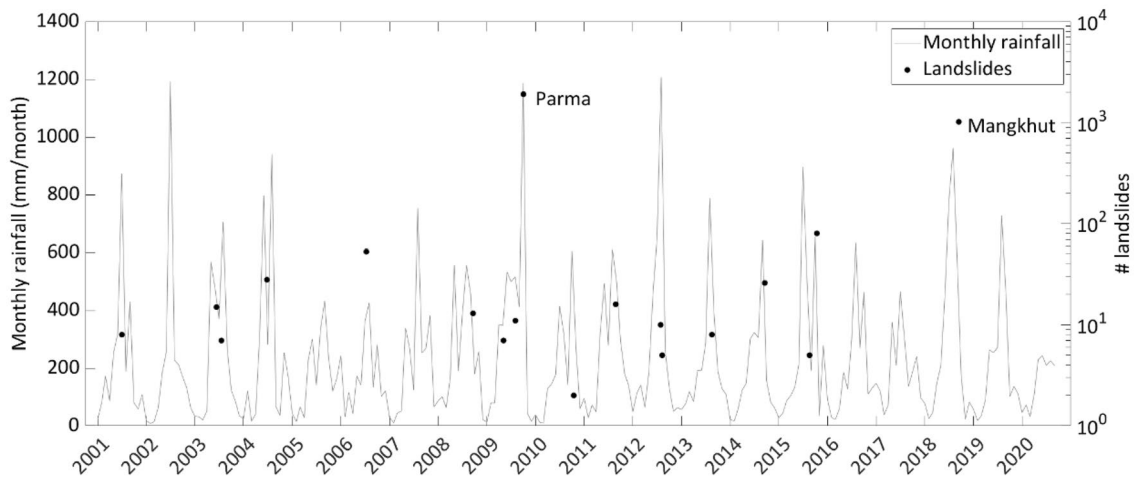


**Fig. 2** Typhoons that caused landslides in the area within the studied period (2001–2020), and the number of known landslides according to available inventories and records. Note that the area considered may slightly vary depending on the source of information (inventories vs. reports)

The friction angle, cohesion, permeability, porosity and density values were determined by few available laboratory tests (Casinal and Ganiban 2021) and estimations based on soil descriptions (Carating et al. 2014) in the other cases. Soil thickness values were initially estimated based on field observations (for example, in the location of Fig. 4) and calibrated in the model (see in the “Results” section).

**Land use and land cover**

The land use and land cover map was provided by the National Mapping and Resource Information Authority of the Philippines (DENR-NAMRIA 2010). It originally had 11 classes within the study area, which, according to the descriptions, were reclassified into seven (Fig. 5b). Table 2 shows the estimated values of the root cohesion and the curve number (United States Department of Agriculture 1986) of each soil type that is required for the analysis using the physically based model for the susceptibility mapping (Medina et al. 2021).

**Rainfall and soil moisture**

Satellite-derived precipitation data from the Integrated Multi-satellite Retrievals for Global Precipitation Measurement (GPM IMERG) (Huffman et al. 2019) mission was used to analyse the rainfall in the study area along the period 2001–2020. In particular, we used rainfall data from the grid cell centred on 248,953 and 1,809,101 (WGS84/UTM 51N) (see Fig. 1). The data have a resolution of 0.1° (approx.10 km) and a time interval of 30 min. The selection of this specific grid cell to be used for the analysis was based on its proximity to the area with a high density of landslides in the two MORLEs that affected the study area.

The rainfall data was employed for (a) performing an empirical comparison between episodes that did and did not trigger MORLEs, (b) input on the water-balance model, to obtain the fractions of rainfall that result in evapotranspiration/runoff/infiltration, and (c) input of the landslide susceptibility model. In this latest case, interpolation of data from 16 grid cells was used to obtain a rainfall map, as can be seen in detail in (Abancó et al. 2021).

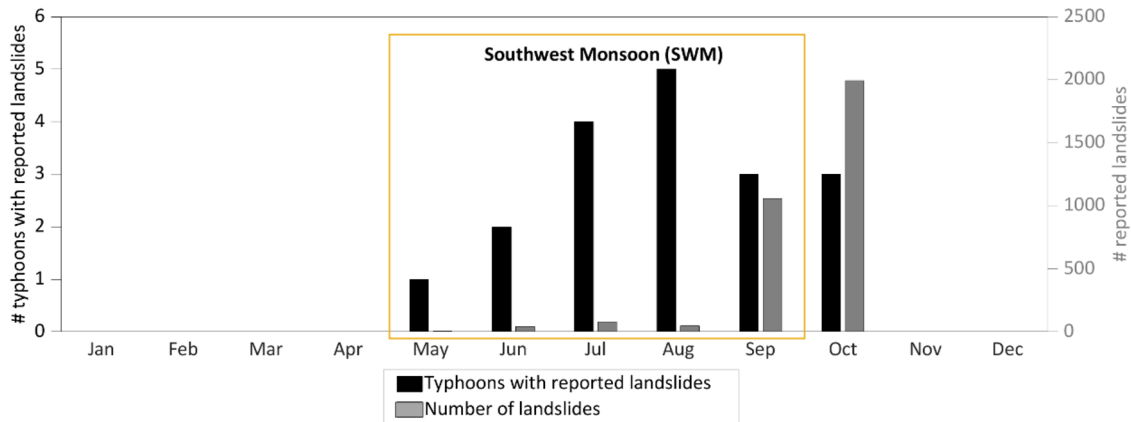


**Fig. 3** Monthly distribution of typhoons and landslides in the study area between 2001 and 2020

**Table 1** Geotechnical properties of the reclassified soil types

Soil type	Permeability (m/s)	Cohesion (kPa)		Friction angle (°)		Soil thickness (m)	Density (kg/m <sup>3</sup> )	Porosity (m <sup>3</sup> /m <sup>3</sup> )
		Min	Max	Min	Max			
<b>Fine (clay, silt)</b>	$1 \times 10^{-6}$	0	5	20	40	2	2000	0.3
<b>Fine-sandy</b>	$1 \times 10^{-5}$	0	3	25	45	2	2000	0.3
<b>Sandy</b>	$1 \times 10^{-4}$	0	3	35	45	2	2000	0.35
<b>Coarse</b>	$1 \times 10^{-3}$	0	2	35	45	2	2000	0.4

We compared the soil moisture obtained by the water balance model (see in the “Water balance mode” section) with the satellite-derived soil moisture data, in particular data from the Soil Moisture Active Passive (SMAP) Level-4 (L4) product (Reichle et al. 2017). Data from SMAP-L4 are derived assimilating previous SMAP products: Level 1, 2 and 3 data, which are processed in a land surface model from NASA. As an input data for the land surface model, the soil porosity is included. The soil porosity is obtained from the Harmonized World Soil Database version 1.21 (HWSD1.21). In particular, for the study area, the soil porosity is 0.47, which is not realistic for a clayey material, as it is further discussed in the Discussion. From all the outputs of the land surface model, we used the “analysis” product, which is an estimate of the 3-hourly instantaneous soil moisture and temperature of the soil. In particular, we used the root zone data (0–100 cm soil layer), which has a spatial resolution of 9 km and a temporal resolution of 3 h.

**Methods**

The influence of the rainfall and soil antecedent hydrological conditions in the triggering of MORLEs has been studied using the coupling of two physically based models, which are explained in detail in the following sections. First, we developed a water balance model to quantify the rainfall infiltration and consequent changes in the soil antecedent hydrological conditions. We applied the water balance model to a 19-year series of rainfall and we empirically compared the soil hydrological conditions and rainfall patterns for different episodes: some that triggered landslides and others that did not. Then, we coupled the water balance model and the slope stability model FSLAM in order to assess the changes in landslide susceptibility due to the changes in soil hydrological conditions along the rainy season of 2018.

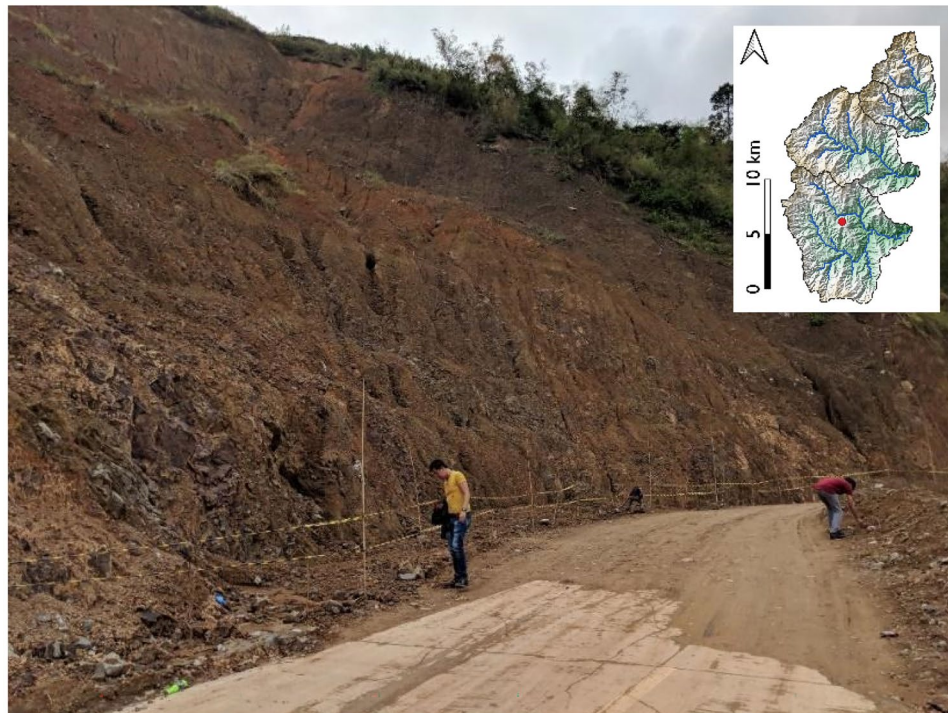


**Fig. 4** View of the slope that was affected by one of the major landslides during Typhoon Mangkhut (2018). Inset, the red dot shows the location of the picture in the study area. Photo credit G. Bennett

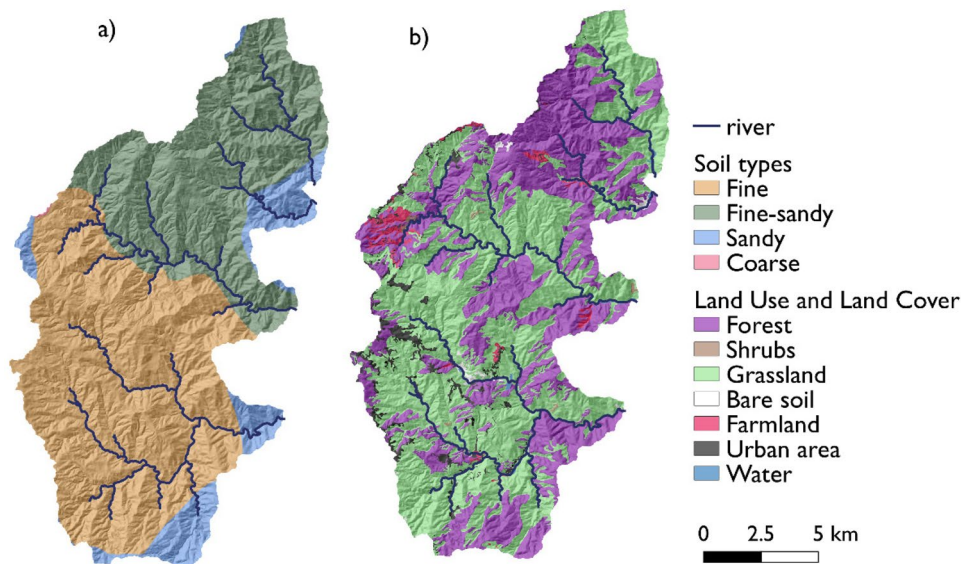


**Fig. 5** Reclassified soil map (a) and reclassified land use and land cover map (b) of the study area

### Water balance model

The water balance model described here is a long-term continuous model (CM) that analyses water movement through the water cycle at daily time steps. Originally, it was developed by UPC BarcelonaTech and called “Easy Bal” model (Serrano-Juan et al. 2020). The original water balance model only included two layers to represent the catchment soil: the root zone and the saturated zone (aquifer). We developed a modified version of the model which includes three layers (Fig. 6) in order to improve the effects of the unsaturated soil conditions. Although the mechanics of unsaturated soil is complex, the proposed model is simplified as we were seeking for a solution that was not computationally expensive and avoids having a lot of input variables. The new model is designed to evaluate water balance per unit of soil area as a function of precipitation, the potential evapotranspiration (or ETP), temperature and irrigation. It physically represents the root zone (Layer 1), unsaturated zone below the root zone (Layer 2) and saturated zone (Layer 3). Layer 2 and Layer

3 have different saturation degrees, but their hydraulic conductivity is the same since they represent the same material type. On the other hand, the bedrock is impermeable.

### Root zone

The hydrological cycle in Layer 1 (root zone) is regulated by the rainfall, the evapotranspiration ( $ETP$ ), the runoff ( $Ru$ ), the infiltration ( $If$ ) and the percolation process from the root zone to Layer 2 ( $Pe$ ). In the root zone, the model consists of six parameters to perform the modelling: latitude, wilting point, initial water content, soil thicknesses, soil porosity, and hydraulic conductivity. The water balance in this layer is based on the following equations.

To estimate potential evapotranspiration, the model uses the Hargreaves method (Hargreaves and Samani 1985), which requires rainfall, maximum and minimum daily temperature data as inputs (Eq. 1).

**Table 2** Land use and land cover

Land use and land cover type	Root cohesion (kPa)		Curve number			
	Min	Max	A	B	C	D
<b>Forest</b>	0	5	30	59	73	79
<b>Shrubs</b>	0	3	32	58	72	79
<b>Grassland</b>	0	2	49	69	79	84
<b>Bare soil</b>	0	3	43	65	76	82
<b>Farmland</b>	0	1	56	68	80	84
<b>Urban area</b>	0	1	90	92	96	98
<b>Water</b>	999	999	100	100	100	100

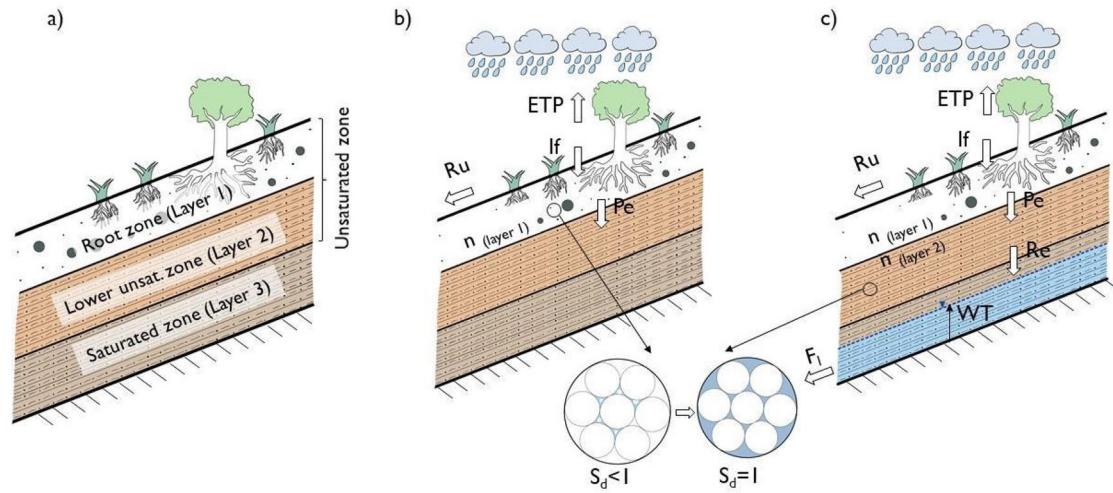


**Fig. 6** Conceptual representation of the three-layer water balance model: structure of the soil before the rain (a); processes occurring in the root zone as the rainfall starts: evapotranspiration (ETP), runoff (Ru), infiltration (If), percolation (Pe) and soil saturation- change in saturation degree ( $S_d$ ) due to reduction of fillable porosity ( $n$ ) (b); processes occurring in the deeper layers as the water infiltrates during the rain: changes in saturation degree, recharge (Re), lateral flow ( $F_l$ ) and increase of the water table (WT) (c)

$$ETP = 0.0023 \times R_a \times (T_{\text{mean}} + 17.8) \times (T_{\text{max}} - T_{\text{min}})^{0.5} \quad (1)$$

where ETP is the potential evapotranspiration in mm/day, and  $T_{\text{mean}}$ ,  $T_{\text{max}}$  and  $T_{\text{min}}$  are the mean, maximum and minimum temperatures, respectively, in Celsius ( $^{\circ}\text{C}$ ). Extra-terrestrial radiation ( $R_a$ ) is estimated based on the location's latitude and the calendar day of the year.

Runoff is calculated by a Hortonian approach. During heavy rainfall, when rainfall intensity exceeds soil infiltration capacity, Hortonian overland flow occurs. It consists of rainfall excess and a recession-infiltration phase. The excess phase has runoff accumulation, while the recession phase sees reduced overland flow as infiltration increases. Hence, a simplistic version to estimate runoff based on the Hortonian approach can be applied in the proposed hydrological model. For instance, when rainfall intensity is greater than hydraulic conductivity (soil permeability), runoff is equal to rainfall at time step  $i$ ; otherwise, all the rainfall infiltrates. It is highly recommended to use hourly rainfall data. Equation 2 can be applied to separate runoff from infiltration (note that  $i$  subindexes refer to timestep):

$$Ru_i = IF(I_i > K, I_i, 0) \quad (2)$$

where  $Ru_i$  and  $I_i$  are the runoff and rainfall intensity at time step  $i$  respectively, and  $K$  is the soil hydraulic conductivity. Therefore, the model can estimate the soil Layer 1 degree of saturation based on the following equation (Eq. 3):

$$S_{d(\text{layer } 1)_i} = \max\left(\min\left(S_{d(\text{layer } 1)_{i-1}} + \frac{(R_{\text{day}} - Ru) - ETP}{n_{i(\text{layer } 1)}}, 1\right), \frac{W_p}{n_{i(\text{layer } 1)}}\right) \quad (3)$$

where  $S_d$  is the saturation degree, the subindex  $i$  indicates time step in days,  $n$  is soil porosity,  $R_{\text{day}}$  is precipitation (mm/day),  $Ru$  is runoff (mm/day),  $W_p$  is the soil wilting point (-),  $n$  is the soil

porosity of layer 1(-) and  $n_i$  (mm) is the total amount of available soil pores obtained by multiplying its porosity and soil thickness. Additionally, volumetric water content (VWC) in this layer can be estimated as (Eq. 4):

$$VWC_i = n_{(\text{layer } 1)} \times S_{d(\text{layer } 1)_i} \quad (4)$$

Finally, the percolation process to the lower unsaturated zone from Layer 1 to Layer 2 ( $Pe$ , in mm) is controlled by the following equation (Eq. 5):

$$Pe_i = (S_{d_{i-1}} - S_{d_i} + \frac{R_{\text{day}} - Ru - ETP}{n_{i(\text{layer } 1)}}) \times n_{i(\text{layer } 1)} \quad (5)$$

#### Lower unsaturated zone

The hydrological cycle in Layer 2 (lower unsaturated zone) is regulated by the percolation from Layer 1 and the recharge process to the saturated zone (recharge to Layer 3). Here, the model considers two parameters: soil thickness and soil porosity. The water balance in this layer is based on the following equations.

Considering Layer 1's infiltration, saturation degree ( $S_d$ ) of the lower unsaturated zone is estimated as (Eq. 6):

$$S_{d(\text{layer } 2)_i} = \min\left(S_{d(\text{layer } 2)_{i-1}} + \frac{(Pe, 0) - Re}{n_{i(\text{layer } 2)}}, 1\right) \quad (6)$$

where  $n_i$  is the total amount of available soil pores of layer 2,  $Pe$  is the percolation from layer 1 (mm) and  $Re$  is the recharge which estimates the amount of water (mm) that is going into the aquifer (Layer 3, saturated zone). The recharge is calculated as (Eq. 7):

$$Re_i = (S_{d(\text{layer } 2)_{i-1}} - S_{d(\text{layer } 2)_i} + \frac{n_{i(\text{layer } 2)} - \max(Pe, 0)}{n_{i(\text{layer } 2)}}) \times n_{i(\text{layer } 2)} \quad (7)$$

### Saturated zone

Layer 3 represents the aquifer and receives water from the unsaturated zone as recharge ( $Re$ ). Water output is calculated as lateral flow ( $F_l$ ) which represents the water that goes into the aquifer. Two parameters control this layer: initial water table and slope. The water balance in Layer 3 is based on the following equations: aquifer water table and lateral flow (mm and mm/day respectively), which are calculated as follows (Eqs. 8 and 9):

$$WT_i = \min\left(\max\left(WT_{i-1} + \frac{Re_{i-1}}{n_{\text{layer } 2}} - \frac{F_{l,i-1}}{n_{\text{layer } 2}}, 0\right), WT_i \times 1000\right) \quad (8)$$

$$F_{l,i} = WT_i \times K \times \frac{\sin(\theta)}{1000} \quad (9)$$

where  $WT_i$  is the water table at  $i$  time step,  $K$  is the hydraulic conductivity (mm/day) and  $\theta$  is the terrain slope (degrees).

### Rainfall and infiltration analysis

The GPM IMERG rainfall data series 2001–2020 was introduced in the water balance model to account for the soil hydrological conditions continuously along the 19 years period. In order to analyse the rainfall and soil hydrological conditions likely to trigger landslides, we developed a code using Matlab (The MathWorks Inc. 2021) to select high-intensity rainfall episodes. The events were selected based on the criteria defined in Abancó et al. (2021): rainfalls with intensity higher than 4 mm/h on average, for 3 consecutive hours. Less than 2% of the 30 min rainfall records exceeded 4 mm/h in the period 2001–2020; therefore, it was considered to be an extreme rainfall intensity. Following Abancó et al. (2021), the start (end) of the rainfall event needs to be preceded (followed) by 1 h without rain.

A total of 561 rainfall episodes were identified, including the episodes with landslides (both MORLEs and other events where less than 100 landslides were reported, so with a density lower than 0.5 landslides/km<sup>2</sup>) (Fig. 7). In particular, three of the rainfall events are associated to MORLEs, and 22 of them to events with less than 100 landslides reported. The rest of the high-intensity rainfall events did not trigger landslides, according to the available records. The reason why three rainfalls are associated to MORLEs while there is only two MORLEs reported in the study area between 2001 and 2020 is because, according to the criteria of start and end of the rainfall event, Typhoon Parma had two different rainfall events: the one starting on the 1st of October 2009 and another one starting on the 5th of October 2009. The second one corresponds to the backward movement of Typhoon Parma after interacting with Typhoon Melor. This also happens with the 16 tropical storms that triggered less than 100 landslides, which resulted in 22 rainfall events.

The result of the analysis was a set of (a) ten parameters that described the characteristics of the event triggering rainfall (duration, event rainfall, mean rainfall intensity, maximum rainfall intensity for 30/60/90/120/180/240/300 min) and (b) five parameters that described the antecedent condition of the soil since the start of the SWM (percolation, accumulated percolation since the start of the SWM, water table, lateral flow, volumetric water content of the root zone soil layer, which is the volume of water per volumetric unit of soil that stays in the root zone).

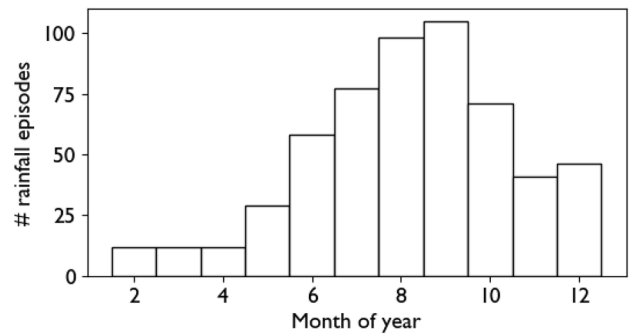


**Fig. 7** Monthly distribution of 561 episodes of high-intensity rainfall registered between 2001 and 2020

### Landslide susceptibility model

The landslide susceptibility model used in this work is the FSLAM model (Medina et al. 2021). FSLAM is a physically based model to assess landslide susceptibility at the regional scale, which main characteristic is its very short computational time. FSLAM consists of a simplified event hydrological model and the infinite slope theory to assess the slope stability. The event hydrological model computes the water table before and after the “event rainfall” (rainfall that triggers the landslides). The factor of safety ( $FoS$ ) is then calculated based on the infinite slope theory, using the geotechnical properties of the soil (the two most sensitive properties can be stochastically included), the slope and depth of the soil layer and the position of the water table. Afterwards, the probability of failure ( $PoF$ ) maps (before and after the triggering rainfall) are calculated based on the stochastic values of the  $FoS$  in each of the cells of the map. A complete description of the model, including the details of the physical background, can be found in (Medina et al. 2021), so will not be repeated here.

We selected three high-intensity rainfall events (“event rainfall”) from the section above to calculate the landslide susceptibility using FSLAM model: two that did not trigger MORLEs and one that happened a month after and did trigger a MORLE. An important point for this work is that FSLAM is a SEM that includes the antecedent conditions as an input, through a parameter called antecedent effective recharge ( $q_a$ ). The antecedent effective recharge in FSLAM is an input of the model and is used to determine the value of the water table at a kind of steady condition before the event rainfall starts. In order to incorporate the transient effect of the soil hydrological conditions along the wet season in this analysis, the water balance model presented above was coupled with FSLAM so the average of 3 months of recharge was used to calculate the antecedent effective recharge and therefore used to calculate the water table.

The coupling of the water balance model and FSLAM was done by using two outputs of the water balance model as inputs in FSLAM. The outputs are (a) the lateral flow ( $F_l$ ), which is the amount of water that goes into the aquifer, and (b) the fillable porosity of the Layer 2 ( $n_{\text{layer } 2}$ ) at the beginning of the landslide-triggering “event rainfall”, which from now on will be referred as  $n_f$ . These two parameters were considered as  $q_a$  (antecedent effective recharge) and  $n$  (porosity) in the geotechnical model of FSLAM,



respectively. FSLAM has a series of inputs that had to be calibrated: the soil geomechanical (cohesion and friction angle) and hydrological (permeability) parameters and the depth of the soil. The calibration process is crucial to make the coupling consistent.

## Results

### Comparison of rainfall patterns and antecedent soil hydrological conditions

Events with multiple landslides happened in the study area in 12 of the 20 years analysed. However, episodes with more than 100 landslides (the threshold used in this study to be considered a MORLE) happened only in two of the 20 years analysed. MORLEs were recorded coinciding with high accumulated rainfall since the start of the southwest monsoon ( $AR_{SWM}$ ), the rainy season, and moderately high daily rainfall ( $R_{day}$ ) (Fig. 8).

The analysis of the 20-year rainfall data series from a GPM-IMERG grid data cell ( $10 \times 10$  km approximately, see Fig. 1 for the location of the grid centre) shows that the majority of the annual rainfall always occurred along the SWM (May to September), when the median monthly rainfall amount is 290 mm/month. In contrast, NEM months (October to April) accumulated less rainfall, with a median value of 65 mm/month. Yearly rainfalls show a large variability, between 1879 and 3746 mm/year, with daily rainfalls as high as 500 mm/day.

Four of the parameters were selected for the analysis of the 561 high-intensity rainfall events (see in the “Rainfall and infiltration

analysis” section) due to their representativity of the antecedent soil hydrological conditions and event rainfall conditions and their presence in the literature: on one side, the percolation since the start of the SWM ( $Pe_{SWM}$ ) and the volumetric water content (VWC) of the soil in the root zone as antecedent water conditions in the soil, and on the other side, the total event rainfall ( $ER$ ) and the maximum hourly rainfall intensity ( $I_{max}$ ) as event rainfall parameters.

Comparing the high-intensity rainfall events, the ones that triggered MORLEs coincide with high values of percolation since the start of the SWM (Fig. 9a, c), with a value of the 96th percentile or higher. Although MORLEs occurred also with the highest values of total event rainfall (97th percentile or higher), the maximum intensities registered in these rainfalls were within the percentile 87th or above, so not extraordinarily high (Fig. 9b). Similarly, when event rainfalls exceed 200 mm (percentile 95th), landslides are very common, but the maximum intensity values are not that representative. Individual landslides can happen even with low values of percolation since the start of the SWM.

The volumetric water content of the soil in the root zone achieves its maximum value very often, as the saturation of the upper layer of the soil is common during the wet season. Although MORLEs happened always in the situation of saturated (or nearly saturated) soil in the root zone, the saturation of this layer of the soil is not a representative parameter to identify landslide occurrence (Figs. 9d, e).

Figure 8b shows that the full saturation of the root zone is very stable during the wet seasons of the period 2001–2020. However, in

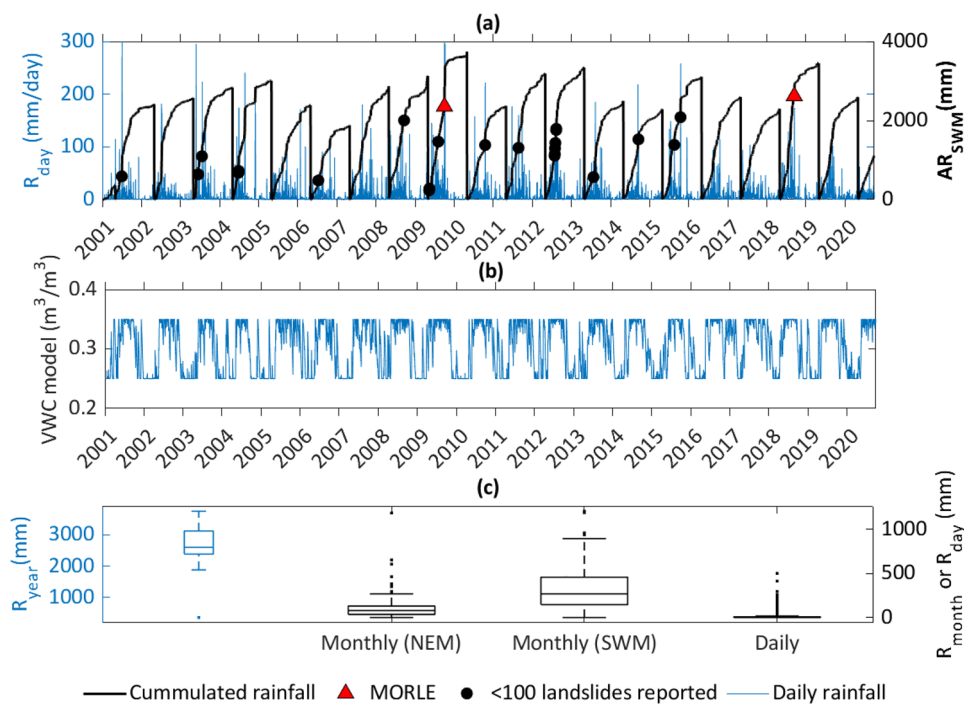


**Fig. 8** Daily ( $R_{day}$ ) and accumulated rainfall since the start of the South West Monsoon ( $AR_{SWM}$ ) for the period 2001–2020 in the study area. Landslide occurrence is indicated, distinguishing between events that triggered more (MORLEs) or less than 100 landslides (a); volumetric water content of the root zone of the soil, calculated using the water balance model (“Water balance model” section) (b); boxplots for yearly, monthly (distinguishing between months of the North East Monsoon, NEM, and South West Monsoon, SWM) and daily rainfall (R) for 2001–2020 in the study area (c)

Fig. 9d, e, it can be observed that saturation of the root zone (VWC values of  $0.35 \text{ m}^3/\text{m}^3$ ) are not a sufficient condition for MORLEs to occur. In contrast, percolation values higher than 1200 mm since the start of the SWM season seem to be a good indicator for MORLEs hazard (Fig. 9a, c).

### Landslide susceptibility assessment

#### Sensitivity analysis of model parameters

The landslide susceptibility model FSLAM has been used in previous studies, although never coupled with the water balance model nor in a tropical climate area. In order to check if the influence of the FSLAM inputs was equivalent to study areas with different climatic contexts and to adjust the range parameter values to this particular case, the process of calibration has been complemented with a sensitivity analysis of the model parameters. The results of the calibration of each FSLAM input parameter based on sensitivity (true positive ratio (TPR)) and specificity (true negative ratio (TNR)) indices are presented. These were obtained using the full inventory dataset. The value range of the input parameters as well as the default values are shown in Table 3. In addition, rainfall event input is usually observed data from rain gauges, radar or remote sensing; therefore, it is assumed as a fixed value.

The results of the sensitivity analysis are plotted by boxplots, and their respective maximum and minimum values are also indicated (Fig. 10). Selected range values for each parameter were chosen considering realistic parameter values for each soil properties input. Seven parameters were evaluated in Fig. 10 where each of

them shows different sensitivity level based on the box height. Furthermore, outliers (showed as points in each extreme of the box-plots) indicate how sensitive a particular parameter value could be when is higher or lower than the average value (median is indicated as a horizontal line in each boxplot).

Results show that one of the most sensitive input parameters is cohesion (Medina et al. 2021; Durmaz et al. 2023) expressed as  $C_s$  and  $C_r$ . The TPR and TNR ranges are significantly larger than the other parameters. The less (more) the cohesion value, the more unstable (stable) the soil, which increases the true positive (negative) ratio allowing to have more landslide (no-landslide) events. They both are the main parameters that control the presence of landslides based on the box width which indicates that, in the assessed parameter range 2.5–25, each iterated value causes a significant change in susceptibility maps (either higher or lower TPR or TNR value).

Parameters  $\log(k)$  and  $\theta$  have similar behaviour in terms of TPR and TNR indices, while  $n$  and  $z$  seem to be parameters with no influence in allowing FSLAM to detect landslides. Only  $z$ , when is set lower than 1 m, shows a big variation in terms of TPR and TNR. Similar to Medina et al. (2021), a particular case is found in  $q_a$  where low values ( $< 1 \text{ mm/day}$ ) are more important than high ones as they do not show a long variation when it is set  $> 1 \text{ mm/day}$ . This is observed as those values are represented as outliers in the boxplot, which indicates that values lower than 1 mm/day cause a variation from 0.7 to 1 approximately for either TPR or TNR; meanwhile, values greater than 1 mm/day only produce a variation from 0.6 to 0.7 approximately. This analysis indicates that  $q_a$  is also one of the most sensitive parameters in FSLAM to produce landslides. In this

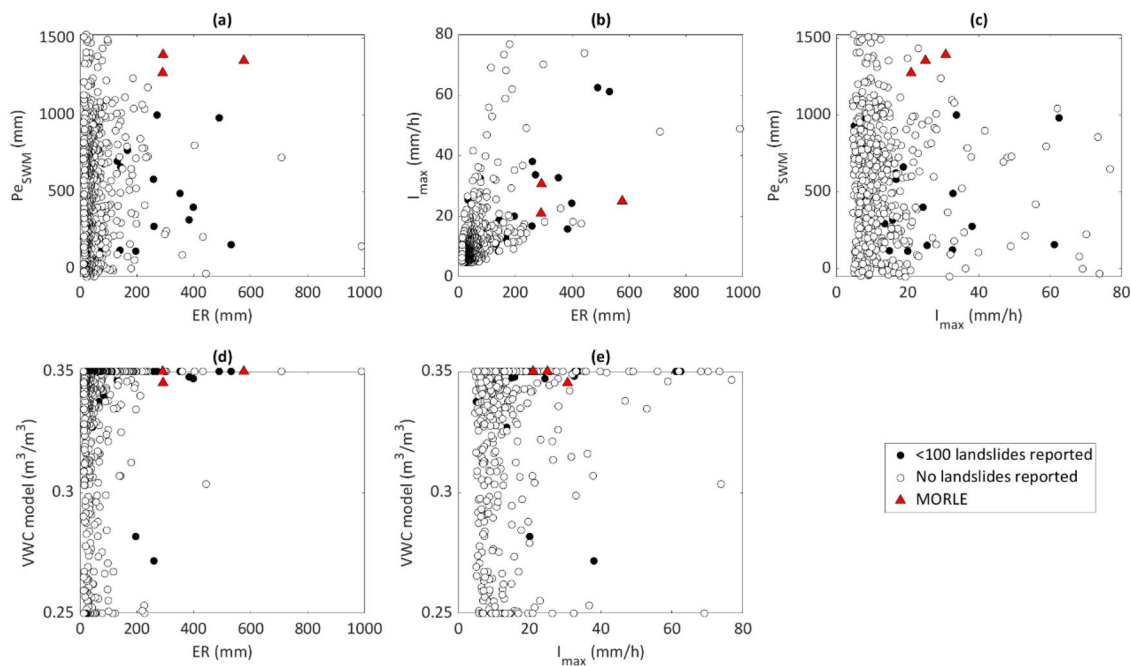


**Fig. 9** Analysis of 561 high intensity rainfalls from the period 2001–2020 in the study area, distinguishing between ones that caused MORLEs, ones that caused landslides (less than 100) and others that did not cause any landslide. Total event rainfall (ER) vs. Percolation since the start of the SWM ( $P_{e_{SWM}}$ ) (a); ER vs. maximum hourly intensity ( $I_{max}$ ) (b);  $I_{max}$  vs.  $P_{e_{SWM}}$  (c); ER vs. volumetric water content of the root zone soil layer (VWC) (d);  $I_{max}$  vs. VWC (e)

**Table 3** Values of input-parameters selected during the model calibration

Input parameter	Parameter name (Medina et al. 2021)	Units	Default value	Minimum value	Maximum value
$C_r$	Root cohesion	kPa	5	2.5	25
$C_s$	Soil cohesion	kPa	5	2.5	25
$\log(k)$	Log hydraulic conductivity	m/s	-6	-7	-5
$n$	Soil porosity	-	0.3	0	0.4
$q_a$	Antecedent effective recharge	mm/day	6	0.1	12
$\theta$ (max)	Soil friction angle	°	40	35	45
$z$	Soil depth	m	1	0.5	5

analysis, it seems that  $q_a$  low values are not suitable if presence of landslides is required in the post-event susceptibility map.

Landslide susceptibility changes at event and seasonal timescales

The comparison of rainfall patterns and soil hydrological conditions (“Comparison of rainfall patterns and antecedent soil hydrological conditions” section) points out that the amount of rainfall infiltrated along the rainy season is a key point in the landslide triggering process. Hence, here we analyse the change of landslide susceptibility at two timescales: event and seasonal timescale. For

this, we selected three high-intensity rainfall events (from the 561 analysed in the “Comparison of rainfall patterns and antecedent soil hydrological conditions” section), which correspond to the same rainy season. The selected events are (a) 16th of July 2018, (b) 9th of August 2018 and (c) 13th of September 2018 (Table 4). The first two events do not have landslides reported, while the third one (Typhoon Mangkhut) is associated with a MORLE.

At seasonal timescale, as the total amount of accumulated water percolated below the root zone increases ( $Pe_{SWM}$ ), the fillable porosity of the soil ( $n_f$ ) decreases due to the reduction of pores available to store water (Fig. 11). As a consequence, the amount of water

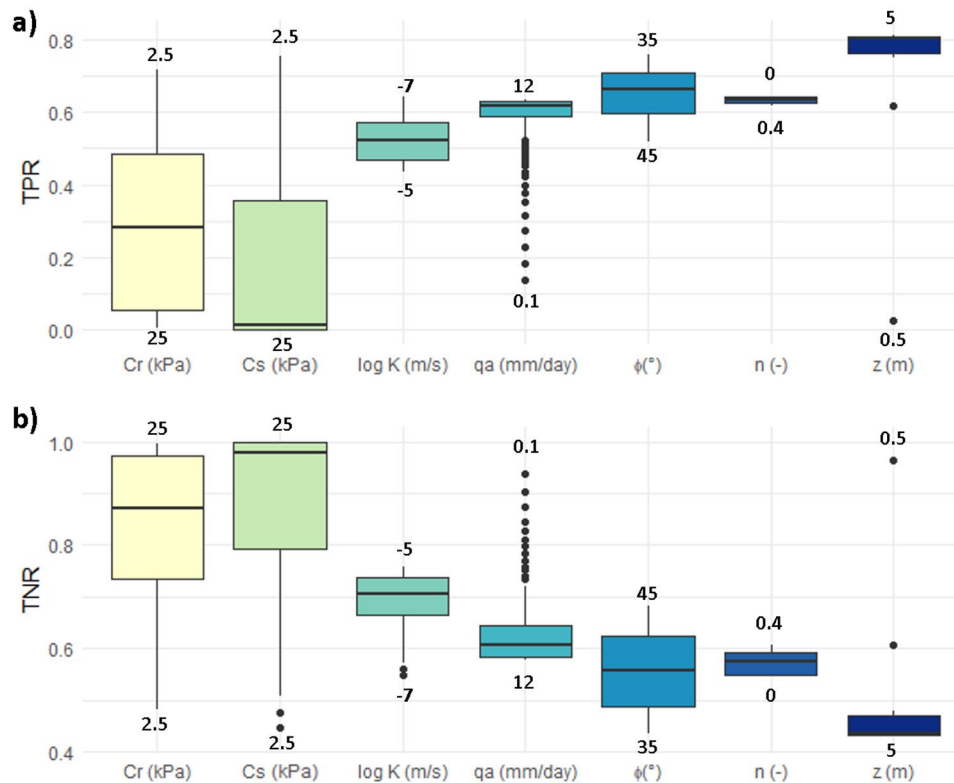


**Fig. 10** Results of the calibration and sensitivity analysis of FSLAM parameters. The two plots present the ranges of TPR (a) and TNR (b) indices

**Table 4** Characteristics of the three selected high-intensity rainfall events for the landslide susceptibility analysis

Date	ER (mm)	$Pe_{SWM}$ (mm)	$I_{max}$ (mm/h)	VWC ( $m^3/m^3$ )	$n_f$ (-)	$q_a$ (mm/day)
16/07/2018	227.3	412.3	16.5	0.35	0.27	0
09/08/2018	402.7	802.4	18.2	0.35	0.18	0.01
13/09/2018	292	1393	30.69	0.35	0.04	0.1

recharging the aquifer increases ( $Re$ ) as the rainy season advances, producing a water table rise. This phenomenon does not necessarily imply a change in landslide susceptibility, as the probability of failure ( $PoF$ ) remains constant until the water table is high enough to drop the factor of safety ( $FoS$ ) values (Medina et al. 2021). In 2018, this situation was not reached until the passage of Typhoon Mangkhut (September 2018); therefore, landslide susceptibility remains nearly constant all along the rainy season until September.

At the event scale, the rainfall is converted into (a) runoff, (b) water to fill in the pores of the unsaturated layers and (c) water that recharges the aquifer producing an increase in the water table. The effect of the “event rainfall” is similar in the July and August scenarios, as the probability of failure ( $PoF$ ) is nearly constant before and after the event rainfall (Fig. 11), meaning that the increase of the water table does not reduce the  $FoS$  to critical levels. In September though, before the passage of Typhoon Mangkhut, the soil in the lower unsaturated zone was very close to saturation (fillable porosity was only 0.04, see Table 4); therefore, the antecedent effective recharge was at its highest levels (0.1 mm/day). With this situation, the event rainfall did generate a water table rise that was critical for many slopes, rising their probability of failure very close to 1 or 1 (Fig. 12). In September, the number of cells with  $PoF$  greater than 0.5 increased by 23% (reaching a value of 26.6%), compared to less than 4% in July and August for the whole area.

The comparison of the situation before and after Typhoon Mangkhut on 15th of September 15, 2018, reveals a significant increase in the probability of failure in the location of the landslides. Before the typhoon, only 5% of the landslide locations had a  $PoF$  (probability

of failure) above 0.5, and 83% had a  $PoF$  below 0.3. However, after the typhoon, 55% of the landslide locations had a  $PoF$  above 0.5, and 65% had a  $PoF$  above 0.3 (Fig. 13). In terms of statistical performance, FSLAM showed an accuracy of 0.63 during this event, where stable cells (no-landslide) were better represented (TNR = 0.73) than the unstable cells (no-landslide) (TPR = 0.54) (Table 5).

## Discussion

Two major topics are discussed in the following. First, the singularities of the landslide hazard assessment in tropical regions will be highlighted, and second, the use of satellite-based soil moisture data for landslide hazard assessment will be debated.

### The singularities of the landslide hazard assessment in tropical regions

In previous studies, Medina et al. (2021) and Hürlimann et al. (2022) applied the FSLAM model to study areas with average annual rainfall from 900 to 1200 mm characterized by an Alpine Atlantic climate and influenced by the Mediterranean Sea and orographic effects. These climates are characterized by high amounts of rain during the summer months, with values of percolation of up to 1 mm/day in the most humid months. In the past analyses of these cases, the simulations with FSLAM associated slope instability with a water table rise during the triggering rainfall, considering that the terrain was already fully saturated. Therefore, the values of 1 mm/day of percolation correspond directly to aquifer recharge.

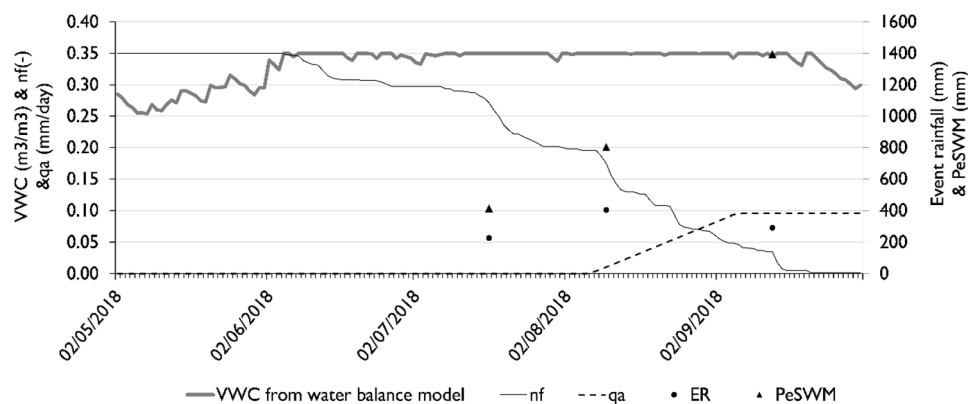


**Fig. 11** Evolution of volumetric water content (VWC), effective porosity ( $n_f$ ), and antecedent effective recharge ( $q_a$ ) along the wet season of 2018. Accumulated percolated water below the root zone along the wet season ( $Pe_{SWM}$ ) and event rainfall (ER) are indicated for the three analysed events

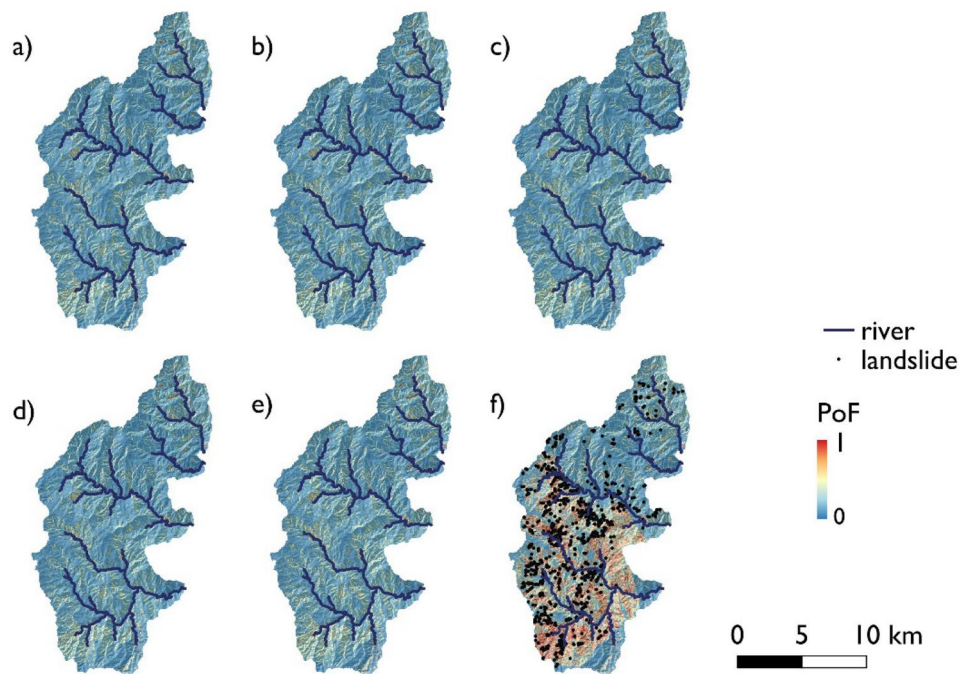


**Fig. 12** Probability of failure map: before (a) and after (d) 16th of July 2018; before (b) and after (e) 9th of August 2018; before (c) and after (f) 13th of September 2018. Landslide inventory is indicated with black dots

In contrast, the climate in the Philippines, with frequent tropical cyclones and two different monsoon regimes, is characterized by percolation rates of up to 20 mm/day in the wet season. With such high percolation rates, if all the water would contribute to aquifer recharge, the water table would rise very quickly and the probability of failure would be continuously very high during the wet season. The reality shows that certain conditions need to be met in order for landslides to happen, as they do not happen every rainy season or with every high-intensity rainfall. Moreover, the initial coupled model (based only on two layers) showed poor performance when considering that all the percolation ( $Pe$ ) is transformed into recharge ( $Re$ ), and therefore, the  $q_{at}$  is very high. Instead, for low values of  $q_{at}$  in the final coupled model (i.e. considering three layers), the results greatly improve (see the “Sensitivity analysis of model parameters” section).

The terrain in the study area is composed of a layer of regolith over unweathered igneous bedrock (mainly diorite), with a weathering degree that gradually decreases in depth from the surface. Although there are some differences between the upper and lower layers of soil due to weathering patterns, the upper 5 m, where landslides occur, display very similar characteristics in terms of hydraulic conductivity and porosity, according to field observations and georadar campaigns. To account for differences in saturation levels between different soil layers (which are represented by fillable porosity), the three-layer water balance model is used. The time it takes for the unsaturated soil to become saturated, begin recharging the aquifer and therefore raising the water table to the point that generates slope instability, depends on the amount of rain that falls during the wet season.

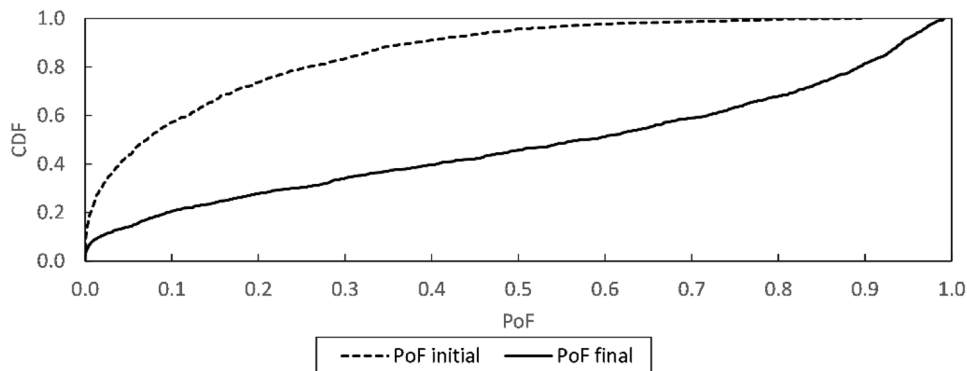


**Fig. 13** Cumulative distribution function (CDF) of the probability of failure (PoF) before and after the 15th of September 2018 in the location of the landslides

**Table 5** Statistical performance of the three rainfall events analysed

Events	Pre-event		Post-event	
	TNR	Accuracy	TPR	TNR
16th of July 2018 (No MORLE)	0.96	-	-	0.94
9th of August 2018 (No MORLE)	0.96	-	-	0.93
13th of September 2018 (MORLE)	0.99	0.63	0.54	0.73

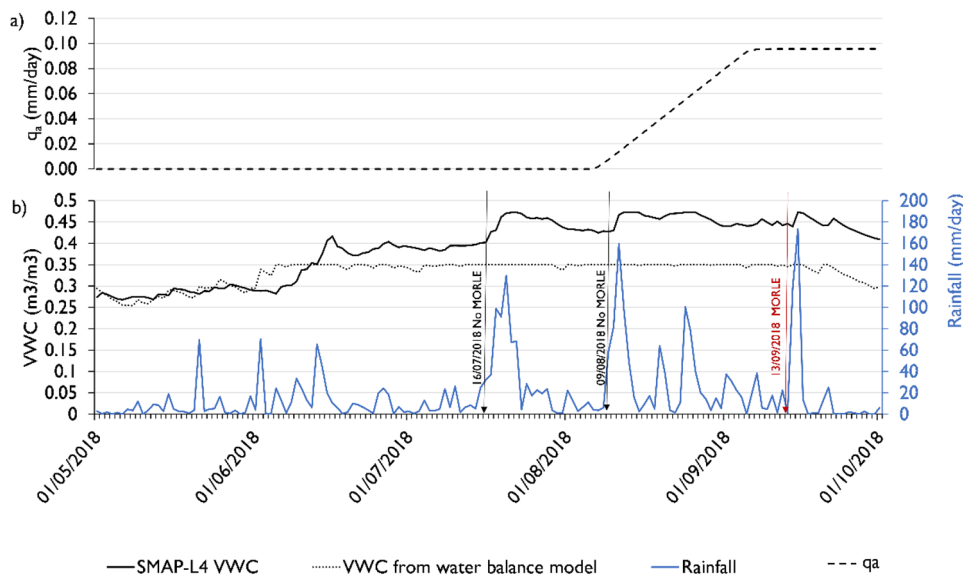
This explains why Nolasco-Javier and Kumar (2018) found that landslides in the area of Baguio are only likely to happen after 500 mm of rain accumulated during the rainy season and why Pelascini et al. (2022) found that typhoon-triggered landslides are likely to happen after consistent rain during the wet season. In order to properly account for all these effects, a water balance model accounting for an unsaturated soil layer below the root zone was developed and coupled to FSLAM. The key point for the landslide hazard assessment in tropical regions is therefore accounting for the change in antecedent soil wetness conditions not only in the root zone but also below it.

#### The use of satellite-based soil moisture data for landslide hazard assessment

The importance of soil water content in the assessment of landslide susceptibility and hazard is a topic that has been raised multiple times in the literature (e.g. Mirus et al. 2018b; Wicki et al. 2020). In fact, recent studies have demonstrated the potential of soil wetness measurements to be included in hydrological-based thresholds to predict regional shallow landslides (Bogaard and Greco 2018; Zhao et al. 2019; Marino et al. 2020; Palau et al. 2023).

In this sense, two-dimensional probabilistic rainfall thresholds are increasing their popularity (e.g. Abraham et al. 2020, 2021; Zhao et al. 2019). These are used as Early Warning Systems to evaluate the conditional probability of the landslide occurrence given the joint occurrence of certain antecedent soil moisture conditions and the severity of a rainfall event. Some of the approaches include soil moisture estimates using satellite-derived data (Brocca et al. 2012; Thomas et al. 2019), while others account for the antecedent soil wetness using physically-based methods (e.g. Zhao et al. 2019). As already mentioned in the introduction, satellite-based data has the advantage of representing a planimetric grid instead of point data (such as the data from in situ sensors), but a main limitation is that data from the satellites is only of the very shallow layer of the soil (< 100 cm).

The present study shows that, in tropical regions, the wetness conditions are very relevant, but in the lower layers of the soil (below the root zone). Therefore, the use of satellite-based soil moisture data for the assessment of landslide hazard assessment would not be sufficient and data in depth is required. For example, in the case of the wet season of 2018 (analysed in the “Landslide susceptibility model” section), soil moisture measured by the SMAP-L4 satellite shows minimal changes from July on (Fig. 14). Here, it is worth pointing out that, as mentioned in the “Rainfall and soil moisture” section, the soil porosity value that is used in the compilation of SMAP-L4 is 0.473. This value is the maximum VWC value for the SMAP-L4 values, but it is not realistic for such fine material as the Bakakeng clay. For this reason, the modelled VWC in the root layer is lower than SMAP-L4 VWC, since it is obtained using a more realistic porosity (0.35). Saturation is reached early in the wet season; however, this is not linked to the triggering of MORLEs. However, starting in mid-August, the recharge of the aquifer starts, as the soil pores of the unsaturated zone (Layer 1 and Layer 2 of the model), are already filled. This element is decisive for the likelihood of landslides to happen, as can be observed with the event on 13/09/2018.

**Fig. 14** Evolution of volumetric water content (b) and antecedent effective recharge ( $q_a$ ) (a) during the wet season of 2018 in the study area

## Conclusions

The main goal of this paper was to understand why regions regularly impacted by typhoons have different slope stability responses under similar rainfall conditions and the same geologic/geomorphologic predisposing factors. We focused on the Itogon region in the Philippines and we studied a 20-year rainfall data series with the objective of comparing the rainfall events that did trigger landslides and the ones that did not, and quantitatively assessing the change of the probability of failure with changes in soil hydrological conditions.

The analysis of 561 high-intensity rainfall events that occurred in the study area showed that the parameter that better identified the critical rainfall was actually the percolation since the start of the wet season (i.e. the South West Monsoon (SWM), from May to October). This parameter represents the amount of water that infiltrates below the root zone and contributes both to saturating the soil and recharging the aquifer (and rising the water table). Rainfall events that had very high intensities occurred at the start of the wet season were not as likely to trigger landslides as the ones that occurred in a more advanced stage of the SWM.

To understand the reason for this phenomenon, we developed a water balance model to track the water cycle into the soil and identify the part that contributes to the soil saturation and the part that leads to a water table rise. This model was afterward coupled with a well-known regional landslide susceptibility model (FSLAM). The resulting coupled model allows the analysis of the transient character of the landslide susceptibility in a simplified way, by using the concept of fillable porosity to represent the process of the soil saturation (see Fig. 11). The simplicity of the model is key to guarantee the computational efficiency and to preserve the idea of FSLAM of being a fast regional physically based model.

The changes in landslide susceptibility are strongly related to the soil antecedent hydrological conditions, in particular to the amount of water that recharges the aquifer, after infiltrating through the unsaturated soil layers. At the beginning of the wet season, the water that infiltrates into the soil contributes to the increase of the saturation degree of the root zone and the lower unsaturated zone but does not contribute to the increase of the water table and probability of slope failure. Only once the soil is saturated the aquifer is recharged and the water table rises, leading to potentially critical situations associated with high-intensity rainfalls.

We conducted an analysis on the evolution of the probability of failure (PoF) in the four sub catchments of our study area during the 2018 rainy season. For this, we studied three episodes of high-intensity rainfall that occurred in July, August and September. During the months of July and August, the probability of failure (PoF) remained almost the same before and after the rainfall event, with an increase of less than 2% and a maximum of 4%. However, in September, the PoF increased by 23%, reaching a value of 26.6%. Additionally, 55% of the landslides that were mapped occurred in areas where PoF values were above 0.5.

The findings of this study suggest that the use of soil moisture satellite-based products for landslide hazard assessment may be insufficient in tropical areas and where an important soil thickness is common. These products are representative of the soil water content in the upper layers of the soil, which we observed were not able to account for the probability of failure of the slopes. The use of physically based models that account for the soil wetness in

lower layers of the soil is, then, more relevant to be used in landslide hazard assessment (e.g. in hydrological-based rainfall thresholds). Soil moisture satellite-based products are best thought as one of the parameters to calibrate the water percolation from the surficial layers into the lower parts of the soil, which leads to instability.

## Acknowledgements

We are thankful to the Goddard Space Flight Center, NASA and National Snow and Ice Data Center for providing free access to GPM IMERG and SMAP datasets. We also extend our thanks to David Hein-Griggs and Adrian J. Matthews for their assistance in the extraction and processing of data. Furthermore, we appreciate the support of Joshua N. Jones, Fabor J. Tan and Mark M. Matera in the analysis of landslides in the Itogon area. We are also thankful to the Mines and Geosciences Bureau (MGB), the National Mapping and Resource Information Authority (NAMRIA) and the Bureau of Soils and Water Management (BSWM) of the Philippines for providing the geological, land use and land cover and soil maps from the Baguio region, as well as the reports of the event in Itogon. We are also thankful to two anonymous reviewers that have greatly helped improving the final manuscript.

## Author contribution

Conceptualization: CA, VM, MH; methodology: CA, FAA, VM, MH; formal analysis and investigation: CA, FAA; writing—original draft preparation: CA, FAA; writing—review and editing: all; funding acquisition: GB.

## Funding

Open Access funding provided thanks to the CRUE-CSIC agreement with Springer Nature. This research has been supported by the Newton Fund (grant no. NE/S003371/1, project: SCaRP).

## Data availability

Landslide inventory is available at: <https://catalogue.ceh.ac.uk/documents/32765a61-8510-4dfc-b7c7-58bad12f8497>. Water balance model and FSLAM model are available at: [https://github.com/EnGeoModels/fslam\\_water\\_balance](https://github.com/EnGeoModels/fslam_water_balance) and <https://github.com/EnGeoModels/fslam>, respectively.

## Declarations

**Competing interests** The authors declare no competing interests.

**Open Access** This article is licensed under a Creative Commons Attribution 4.0 International License, which permits use, sharing, adaptation, distribution and reproduction in any medium or format, as long as you give appropriate credit to the original author(s) and the source, provide a link to the Creative Commons licence, and indicate if changes were made. The images or other third party material in this article are included in the article's Creative Commons licence, unless indicated otherwise in a credit line to the material. If material is not included in the article's Creative Commons licence and your intended use is not permitted by statutory regulation or exceeds the permitted use, you will need to obtain

permission directly from the copyright holder. To view a copy of this licence, visit <http://creativecommons.org/licenses/by/4.0/>.

## References

- Abancó C, Bennett GL, Matthews AJ et al (2021) The role of geomorphology, rainfall and soil moisture in the occurrence of landslides triggered by 2018 Typhoon Mangkhut in the Philippines. *Nat Hazard* 21:1531–1550. <https://doi.org/10.5194/nhess-21-1531-2021>
- Abraham MT, Satyam N, Pradhan B, Alamri AM (2020) Forecasting of landslides using rainfall severity and soil wetness: a probabilistic approach for Darjeeling Himalayas. *Water* 12(3):804. <https://doi.org/10.3390/w12030804>
- Abraham MT, Satyam N, Rosi A, Pradhan B, Segoni S (2021) Usage of antecedent soil moisture for improving the performance of rainfall thresholds for landslide early warning. *CATENA* 200:105147. <https://doi.org/10.1016/j.catena.2021.105147>
- Alonso EE, Gens A, Josa A (1990) A constitutive model for partially saturated soils. *Geotechnique* 40:405–430. <https://doi.org/10.1680/geot.1990.40.3.405>
- Asuncion JF, Jose AM (1980) A study of the characteristics of the northeast and southwest monsoons in the Philippines. NRCP Assisted Project, p 49 (available from the Philippine Atmospheric Geophysical and Astronomical Services Administration, Quezon City, Philippines)
- Baeza C, Corominas J (2001) Assessment of shallow landslide susceptibility by means of multivariate statistical techniques. *Earth Surf Process Landf* 26(12):1251–1263. <https://doi.org/10.1002/esp.263>
- Basconcillo J, Moon IJ (2021) Recent increase in the occurrences of Christmas typhoons in the Western North Pacific. *Sci Rep* 11:1. <https://doi.org/10.1038/s41598-021-86814-x>
- Baum RL, Savage WZ, Godt JW (2008) TRIGRS—a Fortran program for transient rainfall infiltration and grid-based regional slope-stability analysis, Version 2.0. US Geological Survey Open-File Report 2008-1159, p 75
- Bogaard T, Greco R (2018) Invited perspectives: hydrological perspectives on precipitation intensity-duration thresholds for landslide initiation: proposing hydro-meteorological thresholds. *Nat Hazard* 18:31–39. <https://doi.org/10.5194/nhess-18-31-2018>
- Bordoni M, Vivaldi V, Lucchelli L et al (2021) Development of a data-driven model for spatial and temporal shallow landslide probability of occurrence at catchment scale. *Landslides* 18(4):1209–1229. <https://doi.org/10.1007/s10346-020-01592-3>
- Brocca L, Melone F, Moramarco T (2008) On the estimation of antecedent wetness conditions in rainfall–runoff modelling. *Hydrol Process* 22:629–642. <https://doi.org/10.1002/hyp.6629>
- Brocca L, Ponzi F, Moramarco T et al (2012) Improving landslide forecasting using ASCAT-derived soil moisture data: a case study of the torgiannetto landslide in central Italy. *Remote Sens* 4(5):1232–1244. <https://doi.org/10.3390/rs4051232>
- Carating RB, Galanta RG, Bacatio CD (2014) *The soils of the Philippines*. Springer, Netherlands, Dordrecht
- Casingal MM, Ganiban JDU (2021) Slope stability analysis of rainfall-triggered landslides on soft and rocky soils in Itogon. Mapúa University, Benguet
- Chiang SH, Chang KT (2011) The potential impact of climate change on typhoon-triggered landslides in Taiwan, 2010–2099. *Geomorphology* 133(3–4):143–151. <https://doi.org/10.1016/j.geomorph.2010.12.028>
- Crozier MJ (1999) Prediction of rainfall-triggered landslides: a test of the antecedent water status model. *Earth Surf Process Landf* 24(9):825–833. [https://doi.org/10.1002/\(SICI\)1096-9837\(199908\)24:9%3C825::AID-ESP14%3E3.0.CO;2-M](https://doi.org/10.1002/(SICI)1096-9837(199908)24:9%3C825::AID-ESP14%3E3.0.CO;2-M)
- Crozier MJ (2005) Multiple-occurrence regional landslide events in New Zealand: hazard management issues. *Landslides* 2:247–256. <https://doi.org/10.1007/s10346-005-0019-7>
- Crozier MJ (2017) A proposed cell model for multiple-occurrence regional landslide events: implications for landslide susceptibility mapping. *Geomorphology* 295:480–488. <https://doi.org/10.1016/j.geomorph.2017.07.032>
- Crozier MJ, Eyles RJ (1980) Assessing the probability of rapid mass movement. 3rd Australia - New Zealand Conference on Geomechanics, Wellington
- De Vita P, Piscopo P (2002) Influences of hydrological and hydrogeological conditions on debris flows in peri-Vesuvian hillslopes. *Nat Hazards Earth Syst Sci* 2:27–35. <https://doi.org/10.5194/nhess-2-27-2002>
- Department of Environment and Natural Resources-Mines and Geosciences Bureau DENR-MGB (1995) Geological Map of Baguio City Quadrangle (1:50000), Sheet 3169 III, Quezon City, Philippines
- Department of Environment and Natural Resources-Mines and Geosciences Bureau DENR-MGB (2000) Geological Map of Sison Quadrangle (1:50000), Sheet 3168 IV, Quezon City, Philippines
- Department of Environment and Natural Resources-National Mapping and Resource Information Authority- DENR-NAMRIA (2010) Land Cover Map, Taguig City, Philippines
- Durmaz M, Hürlimann M, Huvaj N, Medina V (2023) Comparison of different hydrological and stability assumptions for physically-based modeling of shallow landslides. *Eng Geol* 323:107237. <https://doi.org/10.1016/j.enggeo.2023.107237>
- Emberson R, Kirschbaum DB, Amatya P et al (2022) Insights from the topographic characteristics of a large global catalog of rainfall-induced landslide event inventories. *Nat Hazard Earth Syst Sci* 22(3):1129–1149. <https://doi.org/10.5194/nhess-22-1129-2022>
- Fan L, Lehmann P, Zheng C, Or D (2020) Rainfall intensity temporal patterns affect shallow landslide triggering and hazard evolution. *Geophys Res Lett* 47(1):1–9. <https://doi.org/10.1029/2019GL085994>
- Froude MJ, Petley DN (2018) Global fatal landslide occurrence from 2004 to 2016. *Nat Hazard Earth Syst Sci* 18(8):2161–2181. <https://doi.org/10.5194/nhess-18-2161-2018>
- Gariano SL, Guzzetti F (2016) Landslides in a changing climate. *Earth Sci Rev* 162:227–252. <https://doi.org/10.1016/j.earscirev.2016.08.011>
- Glade T, Crozier M, Smith P (2000) Applying probability determination to refine landslide-triggering rainfall thresholds using an empirical “Antecedent Daily Rainfall Model.” *Pure Appl Geophys* 157(6–8):1059–1079. <https://doi.org/10.1007/s000240050017>
- Grafil L, Castro O (2014) Acquisition of IfSAR for the production of nationwide DEM and ORI for the Philippines under the unified mapping project. *Infomapper* 21(12–13):40–43
- Guo Z, Torra O, Hürlimann M et al (2022) FSLAM: a QGIS plugin for fast regional susceptibility assessment of rainfall-induced landslides. *Environ Model Softw* 150:105354. <https://doi.org/10.1016/J.ENVSOF.2022.105354>
- Guzzetti F (2021) Invited perspectives: Landslide populations-can they be predicted? *Nat Hazard Earth Syst Sci* 21(5):1467–1471. <https://doi.org/10.5194/nhess-21-1467-2021>
- Guzzetti F, Mondini AC, Cardinali M et al (2012) Landslide inventory maps: new tools for an old problem. *Earth Sci Rev* 112(1–2):42–66. <https://doi.org/10.1016/j.earscirev.2012.02.001>
- Guzzetti F, Reichenbach P, Ardizzone F et al (2006) Estimating the quality of landslide susceptibility models. *Geomorphology* 81(1–2):166–184. <https://doi.org/10.1016/j.geomorph.2006.04.007>
- Guzzetti F, Reichenbach P, Cardinali M et al (2005) Probabilistic landslide hazard assessment at the basin scale. *Geomorphology* 72(1–4):272–299. <https://doi.org/10.1016/j.geomorph.2005.06.002>
- Hargreaves GH, Samani ZA (1985) Reference crop evapotranspiration from temperature. *Appl Eng Agric* 1(2):96–99
- Hearn GJ, Hart AB (2019) Landslide susceptibility mapping: a practitioner's view. *Bull Eng Geol Environ* 78(8):5811–5826. <https://doi.org/10.1007/s10064-019-01506-1>
- Huffman GJ, Stocker EF, Bolvin DT, Nelkin EJ, Tan J (2019) GPM IMERG final precipitation L3 half hourly 0.1 degree x 0.1 degree V06 (GPM\_3IMERGHH). Goddard Earth Sciences Data and Information Services Center. <https://doi.org/10.5067/GPM/IMERG/3B-HH/06>
- Hürlimann M, Guo Z, Puig-Polo C, Medina V (2022) Impacts of future climate and land cover changes on landslide susceptibility: regional scale modelling in the Val d’Aran region (Pyrenees, Spain). *Landslides* 19(1):99–118. <https://doi.org/10.1007/s10346-021-01775-6>



- Iverson RM (2000) Landslide triggering by rain infiltration. *Water Resour Res* 36:1897–1910. <https://doi.org/10.1029/2000WR900090>
- Jones JN, Bennett GL, Abancó C et al (2023) Multi-event assessment of typhoon-triggered landslide susceptibility in the Philippines. *Hazards Earth Syst Sci* 23:1095–1115. <https://doi.org/10.5194/nhess-23-1095-2023>
- Jones JN, Boulton SJ, Bennett GL et al (2021) Temporal variations in landslide distributions following extreme events: implications for landslide susceptibility modeling. *J Geophys Res Earth Surf* 126(7):1–26. <https://doi.org/10.1029/2021JF006067>
- Kirschbaum D, Stanley T (2018) Satellite-based assessment of rainfall-triggered landslide hazard for situational awareness. *Earths Future* 6:505–523. <https://doi.org/10.1002/2017EF000715>
- Kirschbaum D, Stanley T, Zhou Y (2015) Spatial and temporal analysis of a global landslide catalog. *Geomorphology* 249:4–15. <https://doi.org/10.1016/j.geomorph.2015.03.016>
- Leonarduzzi E, McArdell BW, Molnar P (2021) Rainfall-induced shallow landslides and soil wetness: comparison of physically based and probabilistic predictions. *Hydrol Earth Syst Sci* 25:5937–5950. <https://doi.org/10.5194/hess-25-5937-2021>
- Lin L, Lin Q, Wang Y (2017) Landslide susceptibility mapping on a global scale using the method of logistic regression. *Nat Hazard Earth Syst Sci* 17(8):1411–1424. <https://doi.org/10.5194/nhess-17-1411-2017>
- Lombardo L, Opitz T, Huser R (2019) Numerical recipes for landslide spatial prediction using R-INLA: a step-by-step tutorial. *Spatial modeling in GIS and R for earth and environmental sciences*. Elsevier, pp 55–83. <https://doi.org/10.1016/B978-0-12-815226-3.00003-X>
- Ma S, Shao X, Xu C et al (2021) MAT.TRIGRS (V1.0): a new open-source tool for predicting spatiotemporal distribution of rainfall-induced landslides. *Natural Hazards Research* 1:161–170. <https://doi.org/10.1016/j.nhres.2021.11.001>
- Marino P, Peres DJ, Cancelliere A et al (2020) Soil moisture information can improve shallow landslide forecasting using the hydrometeorological threshold approach. *Landslides* 17:2041–2054. <https://doi.org/10.1007/s10346-020-01420-8>
- Medina V, Hürlimann M, Guo Z et al (2021) Fast physically-based model for rainfall-induced landslide susceptibility assessment at regional scale. *Catena* 201:105213. <https://doi.org/10.1016/j.catena.2021.105213>
- Melillo M, Brunetti MT, Peruccacci S et al (2018) A tool for the automatic calculation of rainfall thresholds for landslide occurrence. *Environ Model Softw* 105:230–243. <https://doi.org/10.1016/j.envsoft.2018.03.024>
- Mirus BB, Becker RE, Baum RL, Smith JB (2018a) Integrating real-time subsurface hydrologic monitoring with empirical rainfall thresholds to improve landslide early warning. *Landslides* 15(10):1909–1919. <https://doi.org/10.1007/s10346-018-0995-z>
- Mirus B, Morphew M, Smith J (2018b) Developing hydro-meteorological thresholds for shallow landslide initiation and early warning. *Water (basel)* 10:1274. <https://doi.org/10.3390/w10091274>
- Montgomery DR, Dietrich WE (1994) A physically based model for the topographic control on shallow landsliding. *Water Resour Res* 30(4):1153–1171. <https://doi.org/10.1029/93WR02979>
- Napolitano E, Fusco F, Baum RL, Godt JW, De Vita P (2016) Effect of antecedent hydrological conditions on rainfall triggering of debris flows in ash-fall pyroclastic mantled slopes of Campania (southern Italy). *Landslides* 13(5):967–983
- Nolasco-Javier D, Kumar L (2018) Deriving the rainfall threshold for shallow landslide early warning during tropical cyclones: a case study in northern Philippines. *Nat Hazards* 90:921–941. <https://doi.org/10.1007/s11069-017-3081-2>
- Nolasco-Javier D, Kumar L (2019) Frequency ratio landslide susceptibility estimation in a tropical mountain region. *Int Arch Photogramm Remote Sens Spatial Inf Sci* 43:173–179. <https://doi.org/10.5194/isprs-archi-43-XLII-3-W8-173-2019>
- Nolasco-Javier D, Kumar L, Tengonciang AMP (2015) Rapid appraisal of rainfall threshold and selected landslides in Baguio, Philippines. *Nat Hazards* 78:1587–1607. <https://doi.org/10.1007/s11069-015-1790-y>
- Oorthuis R, Hürlimann M, Vaunat J et al (2023) Monitoring the role of soil hydrologic conditions and rainfall for the triggering of torrential flows in the Rebaixader catchment (Central Pyrenees, Spain): role of soil hydrologic conditions and rainfall for torrential flows in the Rebaixader catchment. *Landslides* 20:249–269. <https://doi.org/10.1007/s10346-022-01975-8>
- Palau RM, Berenguer M, Hürlimann M, Sempere-Torres D (2023) Implementation of hydrometeorological thresholds for regional landslide warning in Catalonia (NE Spain). *Landslides*. <https://doi.org/10.1007/s10346-023-02094-8>
- Paringit MCR, Cutora MDL, Santiago EH, Adajar MAQ (2020) Assessment of landslide susceptibility: a case study of carabao mountain in Baguio City. *Int J GEOMATE* 19:166–173. <https://doi.org/10.21660/2020.71.9261>
- Pelascini L, Steer P, Mouyen M, Longuevergne L (2022) Finite-hillslope analysis of landslides triggered by excess pore water pressure: the roles of atmospheric pressure and rainfall infiltration during typhoons. *Nat Hazard* 22:3125–3141. <https://doi.org/10.5194/nhess-22-3125-2022>
- Reichenbach P, Rossi M, Malamud BD et al (2018) A review of statistically-based landslide susceptibility models. *Earth Sci Rev* 180:60–91. <https://doi.org/10.1016/j.earscirev.2018.03.001>
- Reichle R, De Lannoy G, Koster RD et al (2017) SMAP L4 9 km EASE-grid surface and root zone soil moisture geophysical data, version 3. NASA National Snow and Ice Data Center Distributed Active Archive Center, Boulder, Colorado USA. <https://doi.org/10.5067/B59DT1D5UMB4> Accessed: June 2020
- Serrano-Juan A, Criollo Manjarrez RA, Vázquez-Suñé E, Alcaraz M, Ayora C, Velasco Mansilla V, Scheiber Pagès L (2020) Customization, extension and reuse of outdated hydrogeological software. *Geol Acta* 18:0008–0013
- Stanley TA, Kirschbaum DB, Benz G et al (2021) Data-driven landslide now casting at the global scale. *Front Earth Sci (Sec Geohazards Georisks)* 9:1–15. <https://doi.org/10.3389/feart.2021.640043>
- The MathWorks Inc. (2021) MATLAB version: 9.11.0.1769968 (R2021b). <https://www.mathworks.com>. Accessed 1 Jan 2023
- Thomas MA, Collins BD, Mirus BB (2019) Assessing the feasibility of satellite-based thresholds for hydrologically driven landsliding. *Water Resour Res* 55:9006–9023. <https://doi.org/10.1029/2019WR025577>
- Tufano R, Formetta G, Calcaterra D et al (2021) Hydrological control of soil thickness spatial variability on the initiation of rainfall-induced shallow landslides using a three-dimensional model. *Landslides* 18:3367–3380. <https://doi.org/10.1007/s10346-021-01681-x>
- United States Department of Agriculture (1986) Urban hydrology for small watersheds. Technical release 55. National Resources Conservation Service
- van Genuchten MTh (1980) A closed-form equation for predicting the hydraulic conductivity of unsaturated soils. *Soil Sci Soc Am J* 44:892–898. <https://doi.org/10.2136/sssaj1980.03615995004400050002x>
- Wicki A, Jansson P-E, Lehmann P et al (2021) Simulated or measured soil moisture: which one is adding more value to regional landslide early warning? *Hydrol Earth Syst Sci* 25:4585–4610. <https://doi.org/10.5194/hess-25-4585-2021>
- Wicki A, Lehmann P, Hauck C et al (2020) Assessing the potential of soil moisture measurements for regional landslide early warning. *Landslides* 17(8):1881–1896. <https://doi.org/10.1007/s10346-020-01400-y>
- Zhao B, Dai Q, Han D et al (2019) Probabilistic thresholds for landslides warning by integrating soil moisture conditions with rainfall thresholds. *J Hydrol* 574:276–287. <https://doi.org/10.1016/j.jhydrol.2019.04.062>
- Zhuang Y, Xing A, Jiang Y et al (2022) Typhoon, rainfall and trees jointly cause landslides in coastal regions. *Eng Geol* 298:106561. <https://doi.org/10.1016/j.enggeo.2022.106561>

#### Clàudia Abancó (✉)

Departament de Mineralogia, Petrologia i Geologia Aplicada, Facultat de Ciències de la Terra, Universitat de Barcelona, 08028 Barcelona, Spain  
Email: claudia.abanco@ub.edu

#### Flavio Alexander Asurza · Vicente Medina · Marcel Hürlimann

Department of Civil and Environmental Engineering, UPC BarcelonaTECH, 08034 Barcelona, Spain

#### Georgina L. Bennett

Faculty of Environment Science and Economy, University of Exeter, Exeter EX4 4RJ, UK